AD-A238 302

NTATION PAGE

1. Agency Use Only (Leave blank).	2. Report Date. 1990	3. Report Type and Dates Covered. Journal Article

4. Title and Subtitle.
Lamb and creeping waves around submerged spherical shells resonantly excited by sound scattering. II: Further applications

6. Author(s).
G. C. Gaunaurd and M. F. Werby

5. Funding Numbers.
61153N
Program Element No
03202
Project No
010
Task No.
DN255011
Accession No

7. Performing Organization Name(s) and Address(es).

Naval Oceanographic and Atmospheric Research Laboratory
Ocean Acoustics and Technology Directorate
Stennis Space Center, MS 39529-5004

8. Performing Organization Report Number.

JA 221:040:91

9. Sponsoring/Monitoring Agency Name(s) and Address(es).

Naval Oceanographic and Atmospheric Research Laboratory
Basic Research Management Office
Stennis Space Center, MS 29529-5004

10. Sponsoring/Monitoring Agency Report Number.

JA 221:040:91

11. Supplementary Notes.

The Journal of the Acoustical Society of America

12a. Distribution/Availability Statement.

Approved for public release; distribution is unlimited.

12b. Distribution Code.

A-1 20

13. Abstract (Maximum 200 words).

The scattering of plane sound waves from an air-filled steel spherical shell submerged in water in the frequency band $0 < k_1 a < 500$ is studied. This analysis is based on a methodology [Ayres et al., Int. J. Solids Struct. 23, 937-946 (1987) and G. Gaunaurd and M. F. Werby, J. Acoust. Soc. Am. 82, 2021-2033 (1987)] proposed that uses the exact three-dimensional equations of dynamic elasticity to describe the shell motions and to predict its sonar scattering cross section. This approach is valid at all frequencies, for shells of any thickness, of any (constant) curvature, and it accounts for their fluid-loaded condition. The methodology is used to predict the cross sections, which are later interpreted on the basis of the various resonance features that manifest themselves in the frequency response. The spectral locations of these resonances depend on the various types of elastic waves propagating along the shell, or in the surrounding fluid. The exact plots are generated for the phase (c_p) velocities of these (Lamb) waves always accounting for the curvature and fluid-loading effects present on the shell, without appeals to plate waves or theories. Some of the dispersion plots were generated using the Donnell shell-theory approximation, which seems to yield accurate results up to the coincidence frequency. Aside from the broad resonance lobe present at the coincidence frequency frequency, there is another high-frequency resonance lobe, due to a thickness-resonance response curve for a thin shell, around its coincidence frequency, serves to identify the origins of the various types of observed resonance features and to relate them to the elastic and acoustic waves that propagate along the shell or the outer fluid. Many computer-generated graphs are displayed to illustrate the above points.

14. Subject Terms.
acoustic scattering, shallow water, wave propagation

15. Number of Pages.
12

16. Price Code.

17. Security Classification of Report. Unclassified	18. Security Classification of This Page. Unclassified	19. Security Classification of Abstract. Unclassified	20. Limitation of Abstract. SAR

91 6 17 001

DISCLAIMER NOTICE
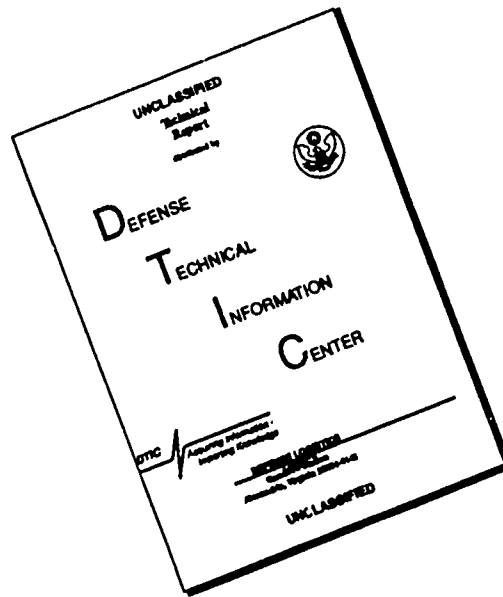
THIS DOCUMENT IS BEST
QUALITY AVAILABLE. THE COPY
FURNISHED TO DTIC CONTAINED
A SIGNIFICANT NUMBER OF
PAGES WHICH DO NOT
REPRODUCE LEGIBLY.

THE JOURNAL
of the
Acoustical Society of America

Lamb and creeping waves around submerged spherical shells resonantly excited by sound scattering. II: Further applications

G. C. Gaunaurd
Naval Surface Warfare Center, White Oak Lab (Code R42), Silver Spring, Maryland 20903-5000

M. F. Werby
Naval Ocean & Atmospheric Research Lab (Code 221), Numerical Modelling Division, Stennis Space Center, Mississippi 39524

The scattering of plane sound waves from an air-filled steel spherical shell submerged in water in the frequency band $0 < k_1 a < 500$ is studied. This analysis is based on a methodology [Ayres *et al.*, Int. J. Solids Struct. 23, 937–946 (1987) and G. Gaunaurd and M. F. Werby, J. Acoust. Soc. Am. 82, 2021–2033 (1987)] proposed that uses the exact three-dimensional equations of dynamic elasticity to describe the shell motions and to predict its sonar scattering cross section. This approach is valid at all frequencies, for shells of any thickness, of any (constant) curvature, and it accounts for their fluid-loaded condition. The methodology is used to predict the cross sections, which are later interpreted on the basis of the various resonance features that manifest themselves in the frequency response. The spectral locations of these resonances depend on the various types of elastic waves propagating along the shell, or in the surrounding fluid. The exact plots are generated for the phase (c_p) velocities of these (Lamb) waves always accounting for the curvature and fluid-loading effects present on the shell, without appeals to plate waves or theories. Some of the dispersion plots were generated using the Donnell shell-theory approximation, which seems to yield accurate results up to the coincidence frequency. Aside from the broad resonance lobe present at the coincidence frequency, there is another high-frequency resonance lobe. due to a thickness-resonance effect, which was also predicted and displayed. A partial-wave analysis of the resonance response curve for a thin shell, around its coincidence frequency, serves to identify the origins of the various types of observed resonance features and to relate them to the elastic and acoustic waves that propagate along the shell or the outer fluid. Many computer-generated graphs are displayed to illustrate the above points.

PACS numbers: 43.30.Ft, 43.30.Gv, 43.40.Qi

INTRODUCTION

The study of the reflection and scattering of sound waves from submerged elastic shells constitutes a problem area not only very rich in scientific and technical challenges but also of crucial importance to our employer in view of its connection with the sensing and the identification of submerged scatterers. Work on this subject started proliferating in the early 1960s,[1,2] and over the years it has included bare[1,2] and coated[3] shells of spherical[1-3] and cylindrical[4] geometries, among others.

The methodology that we will use here to generate our predictions and interpretations is a three-dimensional elasticity approach that first appeared[5,6] in 1987. We will consider Ref. 6 as the first part of this work, hence, its almost identical title. We have worked on this subject over the years,[7-10] using either classical approaches or specific resonance techniques particularly useful in the (broad) resonance region of submerged elastic structures. We have summarized many of our findings[8-10] in reviews that extensively cite the truly large number of contributions to this important area, from all over the world. Of particular importance are a series of monographs[11-16] and papers[17,13] that deal with Rayleigh and Lamb waves. It has become undisputed over

the years that as sound waves impinge on elastic scatterers, the returned echoes have features that depend on the type of elastic waves that get excited on the scatterer. For either an elastic half-space or for an elastic layer of finite thickness, the basic waves are, respectively. the Rayleigh and the (various types of) Lamb[11] waves. For convex solid (or hollow) elastic bodies immersed in fluids these waves have retained their names for the flat case. but have been generalized[12,17] to account for the nonvanishing body curvature. It is in this context that these names are currently used. In spite of the fact that exact three-dimensional descriptors of the shell motions are available,[3,5,6] the tendency to explain features in the sonar cross sections of submerged shells in terms of (loaded or unloaded) *flat plate* waves or theories, still seems to continue. We use the predictions of our approach;[5,6] (i) to explain a variety of new features that have emerged, and (ii) to compare them in some instances to the results obtained from the above mentioned simpler models.

I. THEORETICAL BACKGROUND

The complete classical and RST formulation required for the study of the acoustic echoes scattered from air-filled elastic shells in water has been given in Refs. 5 and 6 for bare

spherical shells, in Ref. 3 for viscoelastically coated spherical shells, in Refs. 4 and 18 for bare cylindrical shells, and in Ref. 19 for viscoelastically coated cylindrical shells. The essentials of this formulation are contained in the form function, which is given by the expression

$$|f_\infty(\theta,x)| = \left| \sum_{n=0}^{\infty} f_n(\theta,x) \right|$$

$$= \left| \frac{2}{ix} \sum_{n=0}^{\infty} (2n+1)A_n P_n(\cos\theta) \right|, \quad (1)$$

where $x = k_1 a$, and the coefficients A_n for the bare, air-filled, spherical shell in water, are given by the ratios of two 6×6 determinants B_n and D_n, viz.,

$$A_n(x) = B_n(x)/D_n(x), \quad (2)$$

where the elements of these determinants are given in Refs. 5 and 6. The outer (or inner) radius of the shell is a (or b).

There are many ways to proceed from here on. Some of these are enumerated below.

(i) *Generation of the backscattering or monostatic form function:* We compute and/or display: $|f_\infty(\theta = \pi,x)|$ vs x. Here we use $P_n(\cos \pi) = (-1)^n$.

(ii) *Isolation of the resonances—spectrogram:* Here we compute and/or display $|f_\infty(\theta = \pi,x) - f_\infty^{(bgr)}(\theta = \pi,x)|$ vs x. The quantity $f_\infty^{(bgr)}(\pi,x)$ is as in Eq. (1) but with A_n replaced by $A_n^{(bgr)}$, where $A_n^{(bgr)}$, for most metal shells in water, is the *rigid* one, given by: $A_n^{(bgr)} = -j_n'(x)/h_n^{(1)'}(x)$. We have often denoted these plots of isolated resonances as the "residual responses" since these residuals constitute what is left of the form function after the suitable backgrounds have been suppressed.

(iii) *The angular scattering pattern at a fixed frequency:* We generate and display $|f_\infty(\theta, x = x_0)|$ vs θ. If x_0 is not a resonance (i.e., a real root of the real characteristic equation $F_n^{-1}(x) = \text{Re}[z_n^{(1)}(x)]^{-1}$), then the resulting plot will be complicated and uninformative. If x_0 is a (real) resonance, then the associated plot displays simplifying and informative features.[8,9]

(iv) *The (bistatic) angular scattering pattern at a fixed frequency, after background subtraction:* The pertinent quantity here is

$$|f_\infty(\theta, x = x_0) - f_\infty^{(bgr)}(\theta, x = x_0)| \text{ vs } \theta.$$

The quantity $f_\infty^{(bgr)}(\theta,x_0)$ is as in Eq. (1), but with $x = x_0 =$ fixed, and A_n replaced by $A_n^{(bgr)}$, as in (ii). What was done above for the summed form function $|f_\infty(\theta,x)|$ can also be done for the partial waves contained within it [viz., $|f_n(\theta,x)|$, for $n = 0, 1, 2, ...$]. This type of partial-wave analysis is very useful and informative.

(v) *Generation of the backscattered partial waves:* Here we compute and display $|f_n(\theta = \pi,x)|$ vs x, for $n = 0, 1, 2, ...$. Again, $P_n(\cos \pi) = (-1)^n$.

(vi) *Resonance isolation within each mode or partial wave of index n:* Here we compute and display $|f_n(\theta = \pi,x) - f_n^{(bgr)}(\theta = \pi,x)|$ vs x in the backscattering direction π, for $n = 0, 1, 2, ...$. Here $f_n^{(bgr)}(\pi,x)$ is as in (ii), with ∞ replaced by the index n.

(vii) *The (bistatic) angular pattern of a single mode n at fixed frequency:* The pertinent quantity is $|f_n(\theta, x = x_0)|$ vs θ, for each value, $n = 0, 1, 2, ...$.

(viii) *The angular scattering pattern of modal resonances:* In this case, we generate and display $|f_n(\theta, x = x_0) - f_n^{(bgr)}(\theta, x = x_0)|$ vs θ, for $n = 0, 1, 2, ...$. Here $f_n^{(bgr)}(\pi,x_0)$ is as in (ii), with ∞ replaced by the index n. If the fixed x_0 is the l th resonance within the mode n, (viz., x_{nl}), then the plot will be proportional to the angular pattern of a Legendre polynomial $|P_n(\cos\theta)|$, and will have $2n$ lobes of different sizes. In the cylindrical case, this plot is proportional to $|\cos n\theta|$, and it still has $2n$ lobes now of equal sizes. Such a plot resembles a "daisy" or a "rosetta." It is a rhodonea of $2n$ petals.

It is often instructive to generate and display calculations versus the modal index n, for fixed values of θ and/or x. A number of relevant cases are as follows.

(ix) *The response surface:* Here we compute the isolated resonances obtained after the subtraction of the appropriate background, and display them versus n and x, in an isometric view. The calculation is done in the backscattering direction $\theta = \pi$ and the pertinent display is $|f_\infty(\theta = \pi,x) - f_\infty^{(bgr)}(\theta = \pi,x)|$, versus n and x. This could also be generated in other directions.[10]

(x) *The spectrogram versus mode order n, at fixed frequencies:* Here we generate and display $|f_\infty(\theta = \pi,x = x_0) - f_\infty^{(bgr)}(\pi,x_0)|$ vs n. The frequency x_0 can be chosen to be a resonance frequency x_{nl} of the body, or not. This is a slice of the response surface in item (ix) at $x = x_0$. Analogously, the spectrogram in item (ii) is a slice of the response surface in item (ix) at each integer value of n.

(xi) *The isolated modal "residuals" displayed versus n at fixed frequencies:* This is analogous to item (x) but for each partial wave or mode n. We generate and display $|f_n(\theta = \pi,x_0) - f_n^{(bgr)}(\theta = \pi,x_0)|$ vs n, at fixed x_0, in the backscattered direction $\theta = \pi$. Here, x_0 can be a body resonance, x_{nl}, or not. This plot shows the strength with which each mode n contributes to the resulting residual, at each chosen frequency x_0.

(xii) *The modal backgrounds in mode-order space n:* These often informative plots show $|f_n^{(bgr)}(\theta = \pi,x_0)|$ vs n, at various fixed $x = x_0$. Clearly, items (xi) and (xii) can be used to display the separation of "backgrounds" and "resonances" in the mode-order domain n. As a companion to item (vi), $|f_n^{(bgr)}(\theta = \pi,x)|$ can also be displayed versus x for $n = 0, 1, 2, ...$ and then such a display, together with item (vi), exhibits the separation of "backgrounds" and "resonances" in the frequency domain, which is standard since the early days of the development of the RST.[8-10]

We have always distinguished the complex eigenfrequencies $\bar{x}_{nl}$, roots of $D_n(\bar{x}) = 0$ in the complex $\bar{x}$ plane, from the real resonances x_{nl}, which are roots of real characteristic equations, which in this case are of the type: $F_n^{-1}(x) = \text{Re}[z_n^{(1)}(x)]^{-1}$. It is at these resonances x_{nl} that peaks and/or dips appear in the plots of the form functions versus the real variable x, and that exactly $n + 1/2$ wavelengths fit the shell's circumference. It is common to also consider an alternative representation in the complex frequency plane $\bar{x}$, and display the complex eigenfrequency there. Both representations have their advantages. The complex eigenfrequencies of a metal shell in water tend to split

into two great groups. One big set, clustered just beneath the Re $\bar{x}$ axis, is associated with the elastic composition of the body. The other large set, arranged in concentric quasisemielliptical loci, and located deeper into the lower half of the $\bar{x}$ plane, is associated with the body shape. To obtain these eigenfrequencies (which approximately have the resonances as real parts) one only needs to solve an equation such as $D_n(x) = 0$ for its roots $\bar{x}_{nl}$, and it is obvious that this can always be done *without* ever having to subtract "backgrounds" as one must do if we look at the frequency dependence of the form function *after the subtraction* of the background [cf. (ii)]. The point here is that once the resonances are found by either approach (viz., either subtracting the appropriate background, or without ever having to talk about backgrounds by solving for the roots of a characteristic equation), they can be used to construct dispersion plots for the phase or group velocities of the (surface) elastic waves that the resonances generate around the scatterer. If we obtain the roots of $D_n(\bar{x}) = 0$ in the (complex) $\bar{x}$ plane, then their real parts turn out to be close to the resonances, and their imaginary parts, to their widths. If the resonances are isolated by means of the spectrogram in item (ii), then their widths can be read from the plot. We repeat that the resonances thus found, *exactly* coincide with the real roots x_{nl} of the (real) characteristic equation $F_n^{-1}(x) = \mathrm{Re}[z_n^{(1)}(x)]^{-1}$. The fact that the Re $\bar{x}_{nl}$ are only approximately equal to the x_{nl} does not imply arbitrariness in the way the x_{nl} are determined.

(xiii) *Dispersion curves for the phase velocities c_l^p of the surface waves:* They are found from the x_{nl} by the relation: $c_l^p/c_1 = x_{nl}/(n + 1/2)$.

(xiv) *Dispersion curves for the group velocities $c_l^{(g)}$ of the surface waves:* They are found from: $c_l^{(g)}/c_1 = 1/\mathrm{Re}[dn_l(x)/dx]$, where c_1 is the sound-speed in the outer medium. Analogous expressions exist[9] for the phase and group attenuation "constants" for the waves revolving around the scatterer.

(xv) *Results in vacuum versus fluid-loaded results:* All the results discussed above are usually found with the exact formulation in Refs. 5 and 6, which accounts for the influence of the outer and inner fluids. A formulation for shells in a *vacuum* could be extracted from the above formulation simply by setting $\rho_1 = 0$ and $\rho_3 = 0$. This would imply that the elements d_{11}, d_{46}, and A_1^* (of Ref. 6) vanish. Such a result would be unrelated to a scattering situation and would be useful only to describe the vibration of unloaded elastic bodies. In this case, it follows that

$$A_n(x) = A_n^{(bkr)}(x)$$

$$= -\frac{j_n'(x)}{h_n^{(1)'}(x)}\underset{x \gg 1}{\longrightarrow}$$

$$\begin{cases} i^n e^{-ix}\cos x & (n = 0,2,4,...) \\ -i^n e^{-ix}\sin x & (n = 1,3,5,...). \end{cases} \quad (3)$$

These shell results account for the precise curvature of the shell in a natural way, whether it is fluid loaded or in a vacuum. It is obvious that if some shell feature such as a branch of a dispersion plot for a phase velocity were to be displayed accounting for, and then ignoring, the fluid-loading effects,

the resulting curves would differ. The two curves would then exhibit a discontinuous "kink" at the point where the fluid-loading condition changes.

(xvi) *Zero-curvature results:* There have been attempts at interpreting features in the scattering cross sections of shells by means of results derived for flat plates. Such attempts may have been motivated by a desire to see how a simpler model could explain a more complex situation that it was not originally meant to explain. It is also conceivable that they may have been due to the difficulty involved in implementing the more general formulation. At high-frequencies, it is possible to estimate the phase velocities for a *shell* (fluid loaded or in vacuum) by their values obtained for a *plate*, by means of the conversion:

$$x = k_1 a \approx \frac{2\pi}{c_1}\frac{(fh)_{n,l}}{1 - b/a}. \quad (4)$$

This relation converted the frequency-thickness products at which certain modes (or branches) occurred in a flat plate, to the $k_1 a$ values for which "corresponding" effects were present for shells. It is at high frequencies that the shell size becomes large compared to a wavelength, and that curvature effects become negligible. The approximation in Eq. (4) fails at low frequencies. The present implementation of shell formulations (cf., Refs. 5 and 6), is valid at all frequencies, and thus, it brings out the features present in all spectral regions.

In what follows, we will always use our shell formulation (Refs. 5 and 6). It will always account for exterior/interior fluid-loading effects, as well as for the precise shell curvatures. The shell deformations are described by the (exact) three-dimensional equations of elasticity—as opposed to the many existing "shell theory" approximations—and it will nowhere need estimates based on flat-*plate* theories or effects. Hence, our results will be valid for all shell thicknesses, curvatures, and in all frequency bands, whether there is fluid loading or not.

In connection to the fluid-loading effects, it has been repeatedly[18] stated that the dispersion curve for the zeroth-order antisymmetric Lamb wave, A_0 propagating in a spherical shell in a fluid starts to be excited for $c_p > c_1$. For $c_p < c_1$ there seems to be no A_0 branch, and what seems to exist then is a section of the dispersion curve corresponding to the "fluid-loaded" case, sometimes called the A branch. This segment seems to be a discontinuous or disjointed extension of the A_0 curve toward the low-frequency end of the spectrum. See below.

In connection to curvature effects it also follows that at low frequencies not only are there resonance effects due to the A_0, A, and S_0 waves, but also to an additional curvature wave. This curvature wave is missed if plate theory approximations are used to predict resonance locations. This wave causes the breathing mode vibration of the shell, and it is the shell counterpart of the interface wave responsible for the giant (monopole, $n = 0$) resonance[9b] of an air bubble in water. For a shell, this resonance is not giant but just large, and it consists of about half a dozen multipole modal components (as can be seen in Fig. 3) or its enlargements. (See the discussion of Fig. 3, below.) Hence, at low frequencies, the general exact three-dimensional shell formulation presented

in Refs. 5 and 6, and implemented here, is the only tool that can accurately examine arbitrary fluid-loading, curvature, and resonance effects in any frequency band of the form functions of submerged shells.

II. NUMERICAL RESULTS AND DISCUSSION

A partial analysis of figures analogous to Figs. 1–3 has already appeared[5,6,18,20-23] in various earlier works. The complete picture that emerges from in-depth studies of these results follows in very abridged form, below. With the exception of our own work,[5,6-8] the form functions have always been analyzed in relative narrow bands not exceeding $k_1 a$ values of 100. We have now extended these bands up to $k_1 a = 500$, which allows us to see some effects never before published, or even noticed.

Figure 1 shows the form function of an air-filled steel shell immersed in water. The relative shell thickness is $h/a = 5\%$. The properties of steel are: $c_{d_2} = 5.95 \times 10^5$ cm/s, $c_{s_2} = 3.24 \times 10^5$ cm/s, $\rho_2 = 7.7$ g/cm^3, and those of water are $c_1 = 1.4825 \times 10^5$ cm/s, $\rho_1 = 1$ g/cm^3. The properties of the internal air are: $\rho_3 = 0.0012$ g/cm^3 and $c_3 = 0.344 \times 10^5$ cm/s. Figure 2 displays the residual response obtained by subtracting the rigid background over the entire spectrum, for the same shell in water in the band $0 < k_1 a < 500$. Figure 3 (top) exhibits the form function of a steel shell of the same properties as before but of thickness $h/a = 2.5\%$, in the band $0 < k_1 a < 100$. The bottom plot shows the *residual response* resulting when we subtract the rigid background throughout the entire spectrum. Dips in the upper plot become resonance peaks in the bottom plot. These curves are obtained by the procedures labeled (i) and (ii) in Sec. I, and the (exact) methodology of Refs. 5 and 6.

Consider Fig. 3 for a steel shell of relative thickness $t \cong h/a = 2.5\%$. There is a clearly visible region of "strong flexures,"[6] or "bump," that starts to develop at $x \sim t^{-1}$, or in this case, for $x \approx 40$. The empirical condition $xt \sim 1$ is a rule of thumb that has emerged from observation of many cases.[6,18] (See, for example, Fig. 4 and its discussion below, for a $t = 5\%$ shell, or Figs. 1–7 of Ref. 6.) It has its origin in the standard coincidence[24] condition $c^p = c_1$ for the A_0 wave. The frequency x, for which $c^p = c_1$ (see, for example, the dispersion plot for A_0 in Fig. 4), seems to always be such that $xt \sim 1$. This condition depends, in general, on material parameters through a proportionality constant C (viz., $Cxt \sim 1$), but for steel $C \cong 0.8$, and thus, it still follows that $xt \sim 1$. Thus, as a rule, the region of strong flexures begins to appear at the coincidence frequency. In addition there are resonance peaks spaced at regular but rather broad intervals throughout the whole spectrum except around the coincidence[5,18,19,21] frequency. Their separation can be read from Fig. 3 to be $\Delta x \sim 3.5$ and they are due to the S_0 wave, which is the only one having its effects felt over the whole spectrum.[5] Then, near coincidence (viz., $40 < k_1 a < 70$), the spacing of the observable resonances becomes smaller (i.e., we read $\Delta x \sim 1.2$) and nearly uniform. These more closely spaced and narrower spikes are due to the A_0 wave, which is almost
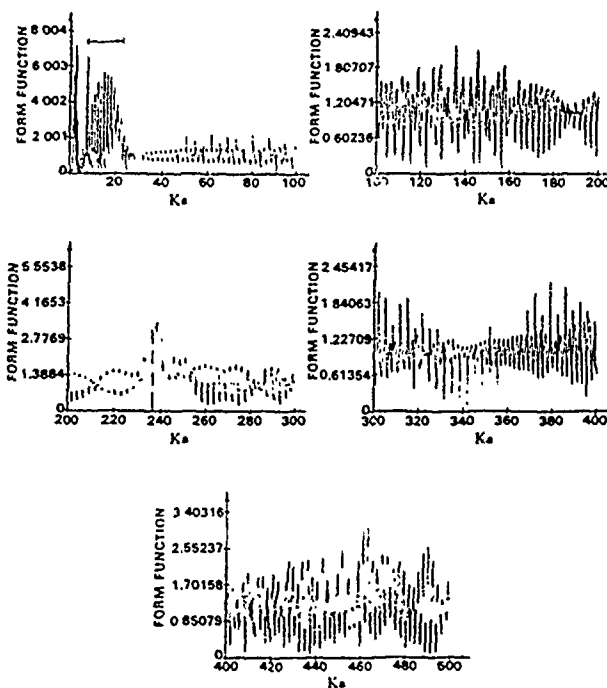
FIG. 1. Form function $|f_\infty|$ as obtained from Eq (1) for a spherical, air-filled steel shell of relative thickness $h/a \equiv 1 - b/a = 5\%$, immersed in water in the (nondimensional) frequency band $0 < k_1 a < 500$.

nondispersive, has lower speed (cf. Fig. 4), and has effects that begin to be felt at coincidence.[5,6] We also note some low-frequency resonance features at $k_1 a \sim 3$, which are due to the nonzero curvature of the shell. For the case of very
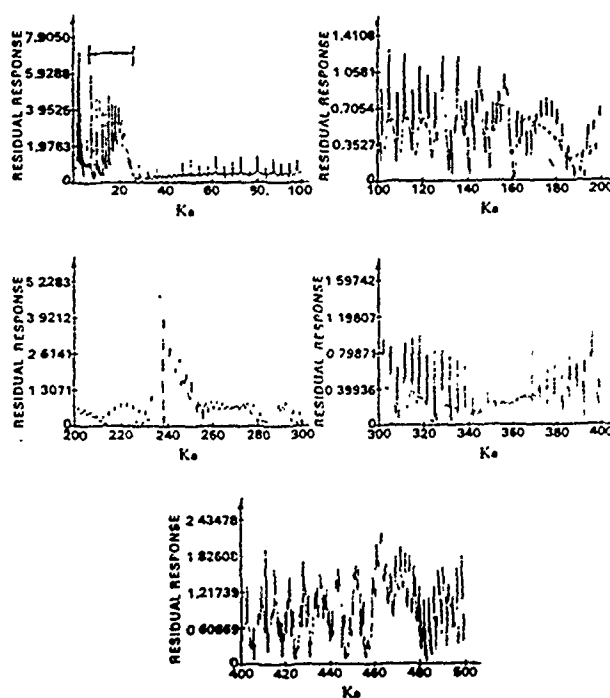
FIG. 2. Residual (or "resonance") response obtained from the form function in Fig. 1 for the same shell, by the subtraction of the (ordinary) rigid background over the entire band $0 < k_1 a < 500$.
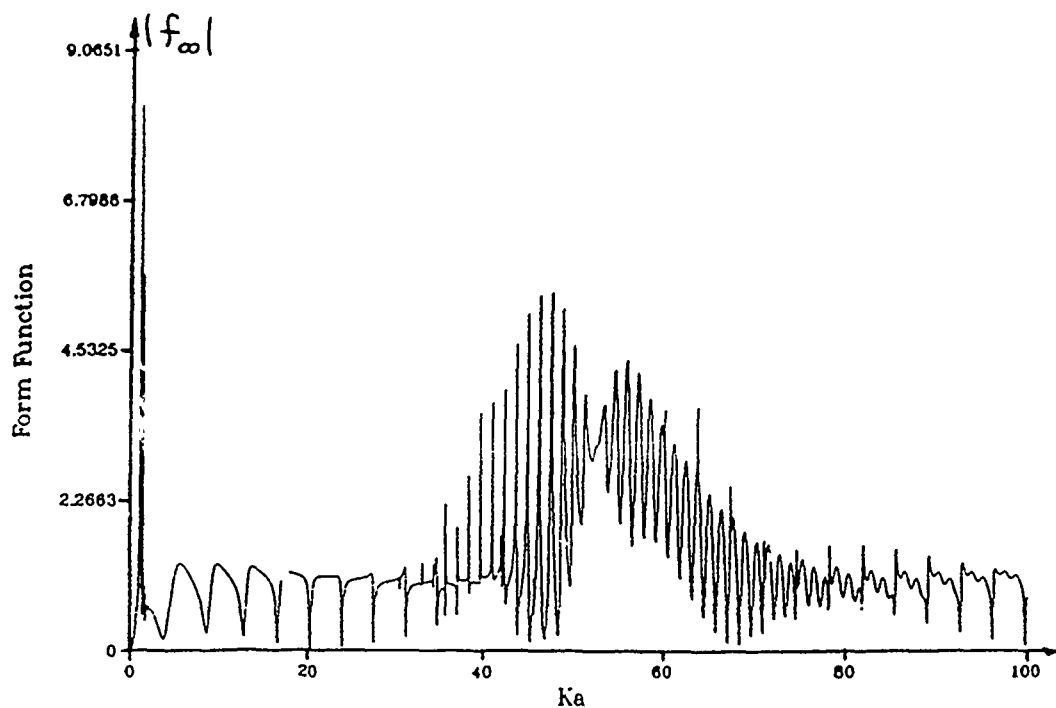
Form Function VS Ka

FIG. 3. Form function (top) and residual response (bottom) obtained by the supression of the rigid background for a steel spherical shell of thickness $h/a \equiv 2.5\%$ in water. These plots show the region of strong flexures around the coincidence frequency, for which $c_p = c_1$.

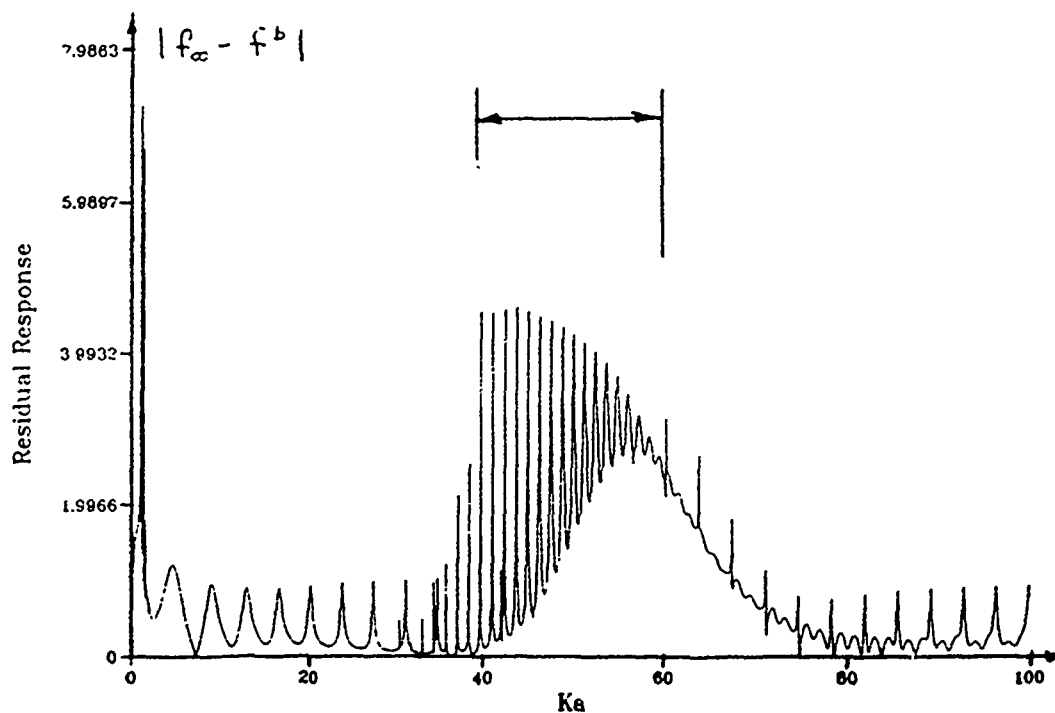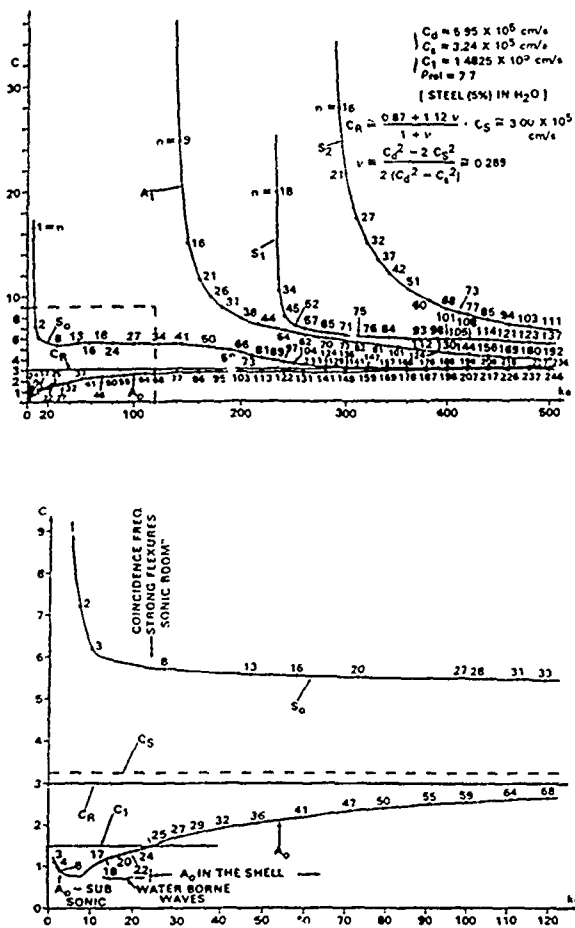FIG. 4 Exact dispersion plots for the phase velocities c_p of the first few symmetric and/or antisymmetric Lamb waves circumnavigating a steel spherical shell of thickness $h/a = 5\%$, in water. The bottom plot is an enlargement of the top one for the low-frequency region enclosed in the dashed-line rectangle. The top graph is the exact spherical counterpart of the often quoted Fig. 26 of Ref. 12, for plates.

thin shells, these resonance features *merge* to produce the (monopole) breathing mode of an air bubble in water, which becomes stronger and eventually giant, the thinner the shell becomes. Figures 1 and 2 also reveal a high-frequency feature (viz., $k_1 a \sim 240$) that had gone unnoticed in the past for shells of this thickness since it appears for $k_1 a > 100$—a region not investigated much in the past. For thinner shells, such a broad resonance occurs at even higher frequencies (viz., at $k_1 a \sim 480$ for $t = 2.5\%$; cf. Fig. 9), as we will see later.

Once we have obtained the resonance locations, we can use them to construct dispersion plots for the phase velocities of the propagating (Lamb) waves. Resonance locations can be read from Fig. 2 or 3 (bottom), or even from Figs. 1 and 3 (top), since in these instances the resonances are quite noticeable even before isolating them by background subtraction. As we mentioned in Sec. I, item (xii), resonance locations can also be obtained by solving for the (real) roots of characteristic equations such as $F_n^{-1}(x)$ $= \mathrm{Re}[z_n^{(1)}(x)]^{-1}$, and then substituting them into the

well-known relation given in item (xiii) of Section I. This alternative procedure does not require background subtraction, but is more computationally intensive. In either case, the result of the analysis for a $t = 5\%$ steel shell in water in the band, $0 \leqslant k_1 a \leqslant 500$, is shown in Fig. 4 (top). A detail of this plot in the low-frequency region (dashed rectangle) is shown in Fig. 4 (bottom). This figure contains much information as we will see below. As mentioned in item (xvi), there have been attempts at interpreting the form-function features of shells in terms of "corresponding" results for flat plates. Consider the often-quoted Fig. 26 of Brekhovskikh's book (Ref. 12) which displays the dispersion plots for the phase velocities of symmetric S_j and antisymmetric A_j ($j = 0,1,2...$) Lamb waves on an aluminum plate in vacuum. Brekhovskikh attributes this figure to Schoch[25] who in turn attrib tes it to Firestone.[26] We have recalculated it for a tungsten carbide plate (Fig. 4, Ref. 5). Many authors have generated it for various metals.[11,13,16,4] That figure shows that at low frequencies, the A_0 branch tends to zero and the S_0 curve approaches a small constant value slightly below the value c_{d_2}/c_{s_2}. Figure 4 is the counterpart of that old plot, now for air-filled steel spherical shells in water. In the band $0 \ll k_1 a \ll 500$, five branches enter the picture, namely A_0, A_1, and S_0, S_1, and S_2. For shells, both the A_0 and the S_0 branches attain very high c values at the low-frequency end of the plot. Having Fig. 4, it is no longer necessary to use flat-plate results (such as Fig. 26 of Ref. 12) to physically interpret resonance features in the backscattering cross sections of fluid-loaded elastic shells. In fact, Fig. 4, which corresponds to the exact solution for a shell treated by three-dimensional elastodynamics, differs substantially at low frequencies from the equivalent (standard) results obtained[12,13] from plate theories. According to the relation in Sec. I (xiii), the phase velocities $c_f^p(x)$ are proportional to the resonances x_{nl}, found as roots of the pertinent characteristic equation. This whole procedure is entirely contained in the frequency domain x, and is unrelated to approaches developed for the mode-order domain. The numbers marked along the various branches of the dispersion curves correspond to values of the index n at the various frequencies at which they occur. These numbers are obtained by carrying on a partial-wave analysis of the form function as indicated in items (v) and (vi) of Sec I, for various values of the mode index n. At high frequencies, the A_0 branch tends to the Rayleigh speed c_R. Figure 4 (bottom) shows that the A_0 branch crosses the $c = c_1$ level at the coincidence frequency, near $x = t^{-1} \approx 20$. For frequencies below coincidence, the A_0 branch is to be replaced by the fluid-loaded branch A, which here is determined from our (exact, 3-D) *shell* formulation,[5,6] not from any flat-plate result.[25,26] Only in this fashion can the shell curvature (as well as fluid loading) effects be preserved and studied. The (sometimes called fluid loaded) A branch is *not* shown here (in Fig. 4), but it is known to remain always "subsonic" $c < c_1$. The term "subsonic," or "supersonic" ($c > c_1$) often used to describe these phase velocities, is to be used with the understanding that there are no perceivable transonic effects or "sonic booms" occurring as these phase velocities exceed the sound speed in the medium. It is known that phase velocities in analogous electromagnet-
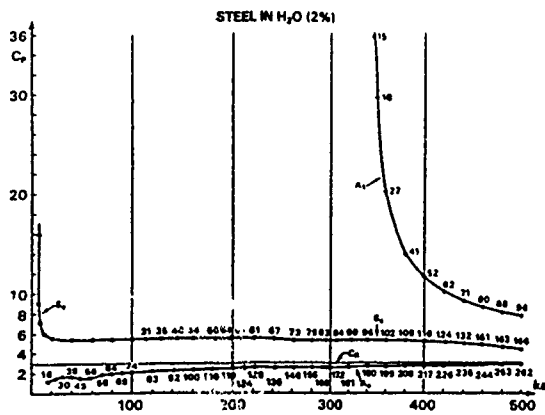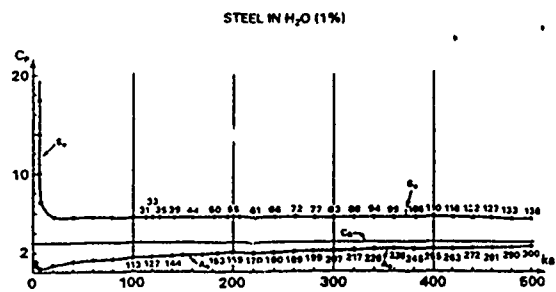
STEEL IN H₂O (2%)

STEEL IN H₂O (1%)

FIG 5. Exact dispersion plots for the phase velocities c_p of the Lamb waves on a water-loaded steel spherical shell of thickness $h/a = 2\%$ in the band $0 < k_1 a < 500$. Three branches of the dispersion curves (viz., those corresponding to the A_0, S_0, and A_1 waves) are present in this band. The numbers along the curves correspond to values of the index n at the various frequencies.

Residual Response VS. Ka

ic instances can even exceed the speed of *light* in the medium in question. The S_0 branch is the exact 3-D elasticity counterpart of Junger's[27] upper branch of eigenfrequencies found by means of Donnell's *shell*-theory equations.[28] At low frequencies, the Donnell theory results do not differ much from the exact 3-D elasticity results given in Fig. 4, for that branch. Note that the exact S_0 branch displayed in Fig. 4 has a relatively flat shape in the enlargement (bottom), but as it is seen in the top graph for $0 < k_1 a < 500$, at the higher frequencies, it bends down and asymptotically approaches c_R, just as the A_0 branch.

Figure 5 displays analogous results for a spherical steel shell in water of thickness $t = 2\%$ in the band $0 < k_1 a < 500$. For this thickness, only three branches of the dispersion curves (viz., A_0, A_1, and S_0) are present. The others appear at still higher frequencies. Figure 6 displays analogous results for the shell in the same band when the thickness is now $t = 1\%$. Only the A_0 and S_0 branches are present in this case. All that was said for the thicker shell still applies for Figs. 5 and 6. The bottom part of Fig. 6 shows a section of the residual response in the high-frequency band $400 < k_1 a < 500$ for a $t = 1\%$ steel shell in water. In general, suppression of the rigid background does not exactly isolate the resonances, everywhere, in a completely clean and clear fashion. The last segment of Fig. 2 ($400 < k_1 a < 500$) for the $t = 5\%$ shell shows the point well. Even though at high frequencies the rigid background should[7] become "better," the last segment of Fig. 2 shows that such is not always the case. Figure 6 (bottom) is displayed here merely to show that if a "modified" background is used, the resonance-isolation process that results is very clean and accurate. The modified background responsible for Fig. 6 does not assume the scatterer rigid as in many earlier RST papers, but it accounts for the matching of elastic properties of the scatterer and the fluid loadings taking place at the shell's surfaces. Its mathemat-

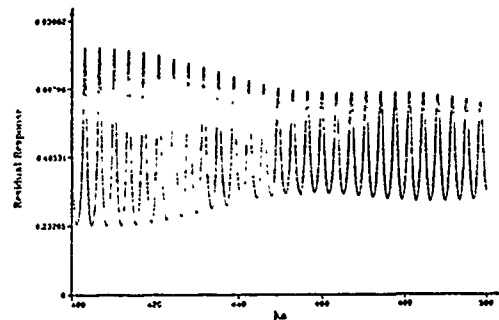ical derivation is lengthy and will appear elsewhere. Simple observation of Fig. 6 is the best evidence of its appropriateness.

Figure 7 shows the dispersion plot for the phase-velocity of the A_0 branch for a steel spherical shell of $t = 1\%$ in water. It coincides almost exactly with the A_0 branch shown in Fig. 6 (top) which was computed using the exact 3-D formulation of Refs. 5 and 6. However, it was calculated here by means of the Donnell shell-theory equations[28] used by Junger and others.[27] This plot is simpler and faster to generate than the one in Fig. 6 (top).

Figure 8 shows the form equation (top) and the residual response (bottom) of a steel shell of $t = 1\%$ in water. The curves are found in the band $300 < k_1 a < 500$, and the lower ones have made use of the "modified" background mentioned above. While the form function (top) exhibits some peaks and some dips, the "residual" response displays clear resonances everywhere. In fact, as stated above, these residuals *are* the isolated resonances, as predicted by the present approach.

Figure 9 is analogous to Fig. 8, but the steel shell now has thickness $t = 2.5\%$. The novelty is the appearance of a large broad peak near $k_1 a \approx 486$. In fact, it extends from $k_1 a = 470$ to 510. This feature was seen earlier at $k_1 a \approx 240$
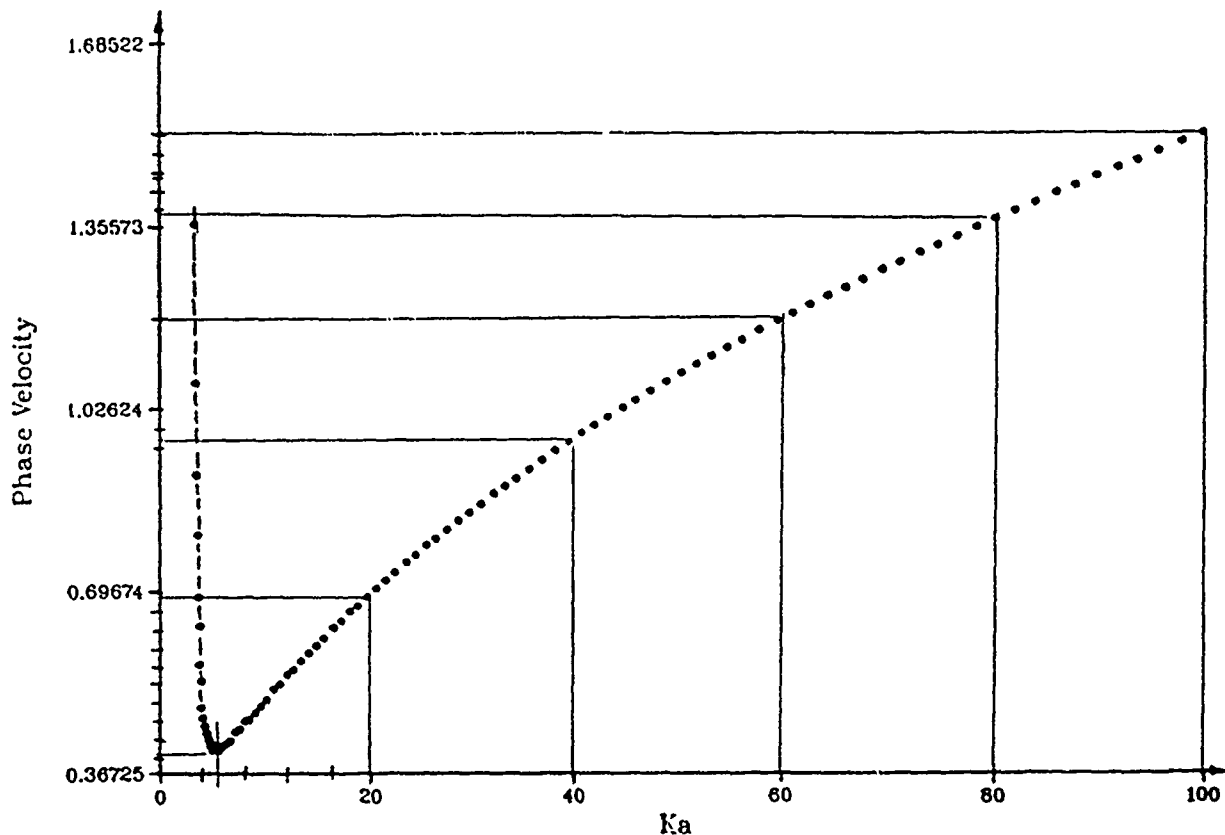
FIG. 7. Detail of the dispersion plot for the phase velocity c_p of the A_0 Lamb wave on a 1% steel shell in water, in the band $0 < k_1 a < 100$.
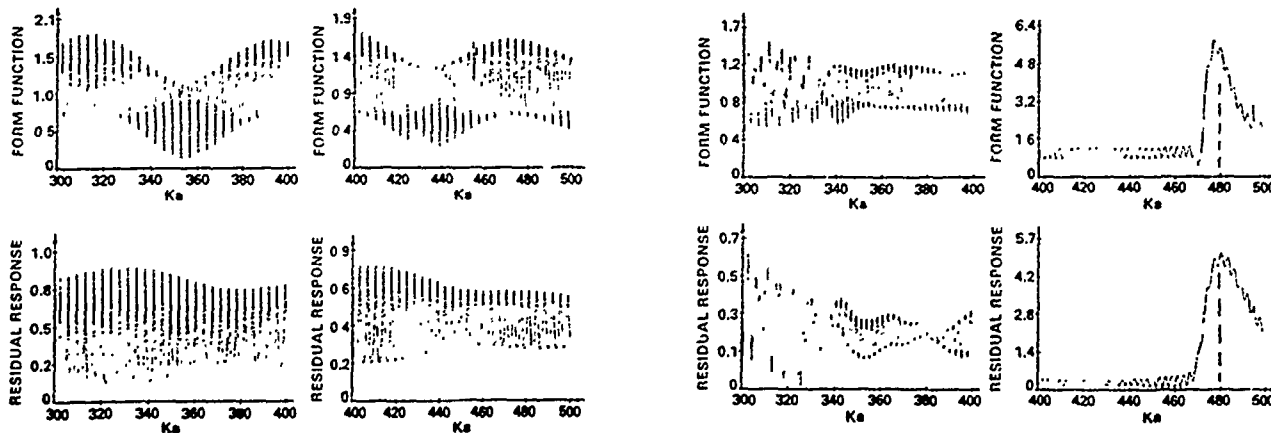
FIG. 8. Form function (top) and residual response (bottom) for a 1% steel shell in water in the band $300 < k_1 a < 500$. We underline the clean and clear nature of the isolated resonances in the bottom plot, obtained via the same "modified" background used in Fig. 6 (ii).
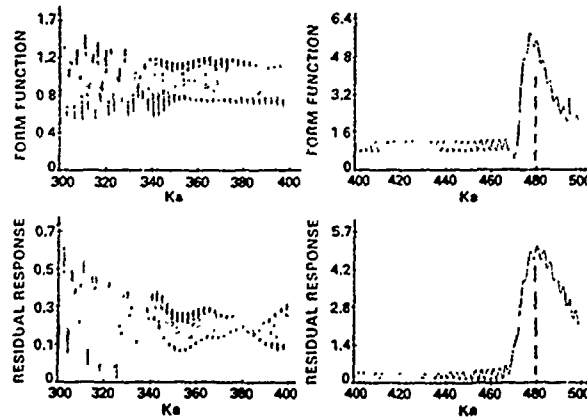
FIG. 9. Same as Fig. 8 but now for a steel shell of thickness 2.5%. The main feature observable in this case is a large and wide resonance peak near $k_1 a \sim 480$. This is caused by a thickness resonance effect resulting when the frequency-thickness product for the shell equals either the phase velocity of the pertinent Lamb wave propagating along the shell, or half the shell's dilatational wave speed.

for a 5% shell in Figs. 1 and 2. Figure 10 displays dispersion plots for the phase velocities of the first three Lamb waves A_0, S_0, and A_1 in the band: $300 < k_1 a < 500$. We note that near 480 the c_p of the A_0 branch is ~ 2.87 Km/s. This new large peak is caused by a *thickness resonance* effect present in the shell which we analyze below. This peak co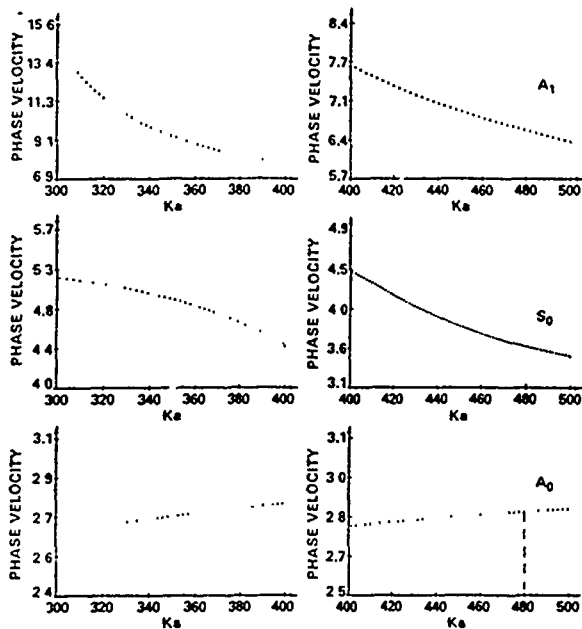uld be caused by the fact that the phase velocity of the propagating wave equals the frequency-thickness product (viz., for $c_p = fh$). This condition is not due to the coincidence phenomenon, although it resembles it in form. In fact, this resonance condition could be simply stated as: $h = \lambda$, where $\lambda = c_p/f$ is the wavelength of the A_0 wave in the shell, of phase velocity c_p. Shell motions in this situation are of a bending or flexural nature, and follow a direction through the thickness, normal to the fluid–solid interface, as one would observe at the incidence point on the shell. Such condition serves to predict the spectral location of the large thickness resonance, since

$$x = k_1 a = \frac{2\pi a}{c_1} f = \frac{2\pi a}{c_1} \frac{c_p}{h} = \frac{2\pi}{c_1} \frac{c_p}{h/a}. \quad (5a)$$

Substitution of the numerical values yields

$$x = \frac{2 \times 3.14 \times 2.87 \times 10^5}{1.4825 \times 10^5 \times 0.025} \approx 480,$$

just as seen in Fig. 9. There is a "principle of transverse resonance"[11,12,14,24] that could also account for this peak, and which is usually written as $h = m\lambda_s/2$ for $m = 2, 4, 6, \ldots$, where λ_s is the shear wavelength in the layer. For $m = 2$, this condition is $h = \lambda_s$; (or equivalently, $k_s h = m\pi$), which differs from the previous resonance condition in that we now have λ_s rather than λ in the right side. This leads to $c_s = fh$ and to an equation to predict the peak location which is

$$x = \frac{2\pi}{h/a} \frac{c_s}{c_1}, \quad (5b)$$

which differs from Eq. (5a) in that c_p is now replaced by c_s. There is also an analogous "principle of longitudinal resonance"[11,12,14,24] usually written as $h = n(\lambda_d/2)$ for $n = 1, 2, 3, \ldots$, where λ_d is the dilatational or longitudinal wavelength in the layer, which is easily seen to be equivalent to $k_d h = n\pi$. For $n = 1$, it leads to $c_d/2 = fh$, or simply, $h = \lambda_d/2$. The peak location could be now predicted by

$$x = \frac{2\pi}{h/a} \frac{c_d}{2c_1}, \quad (5c)$$

which differs from Eq. (5a) in that c_p has been replaced by $c_d/2$. Substituting the values of the material parameters into Eqs. (5b) and (5c) yields

$$x = \frac{6.28 \times 3.24 \times 10^5}{0.025 \times 1.4825 \times 10^5} = 549,$$

for Eq. (5b), and $x = 504$ for Eq. (5c). Figure 9, which displays our numerical prediction, shows the broad thickness peak extending within: $470 < x < 510$, with the top of the peak at ~ 480. This rules out the prediction of Eq. (5b), which is $\sim 13\%$ too large. However, it implies that both Eqs. (5a) and (5c) predict a location for the thickness resonance peak which is in agreement with our calculations in Fig. 9 for a steel shell. In the absence of other evidence, it seems that the prediction of the main peak displayed in Fig. 9 is best given by Eq. (5a); however, that of Eq. (5c) is only $18/504 \cong 3.5\%$ away from the other, and thus, the differences are small. They are close enough to each other to be both "confirmed" by the calculations we have performed for several other thicknesses and materials which will be shown elsewhere. At present, it is not clear if the location of this large thickness resonance peak should be determined by that of its central lobe of highest amplitude, or by that of one of the particular subpeaks that form it (see Fig. 9). This point will be further studied by us in the future. For the case in Fig. 2, the phase velocity is slightly less than the values found here, so the location of the peak in Fig. 2 is about $x \equiv k_1 a \approx 236$, as seen there. Finally, the resonance for a 1% steel shell in water is enlarged in Fig. 11 in the band $90 < k_1 a < 150$. It is in this band that the strong flexures begin to appear at the coincidence frequency $x \approx 100$. This figure was already examined in Fig. 3(c) of Ref. 6; however, now the various peaks in Fig. 11 have been identified with the various mode orders n that cause them. This is done by a partial-wave analysis as described in items (v) and (vi) of Sec. I, and used in Figs. 4–6. This partial-wave analysis shows each one of the individual contributions to the ensemble of peaks appearing in Fig. 11, and permits one to identify them in that fashion. Figure 11 displays the set of resonances numbered $n = 107$ to 126, which are separated a narrow distance $\Delta x \sim 1.2$, and are due to the A_0 wave, which in the present exact formulation, always accounts for fluid loading and shell curvature. It also displays another resonance set, spaced a wider amount, $\Delta x \sim 3.5$, toward the right end of the plot, which is due to the S_0 wave, originally studied by Junger[27] by means of a shell-theory approximation analogous to the one we used in Fig. 7. Coincidence occurs near

$k_1 a \sim 108$. For a $t = 1\%$ shell, it should appear at $x = k_1 a = t^{-1} = 100$ but as we mentioned above, this relation is to be modified by a multiplicative factor that depends on material parameters and that is close to unity. The left portion of Fig. 11, up to $ka \simeq 125$ actually shows the superposition of two resonance families. The flexural (antisymmetric) resonance family begins to appear slightly below the coincidence frequency, at which point, a (forthcoming) partial-wave analysis of the figure shows that the individual resonance contributions are quite broad when displayed versus ka. These flexural contributions are coherent and add in phase below coincidence, but are out of phase above it so that an envelope type of function becomes noticeable. This envelope makes up the "bump" characteristic of this neighborhood of the coincidence frequency. Superimposed on this envelope is a narrow resonance family due to a surface wave analogous to the Stoneley wave at the interface of an elastic plate fluid-loaded on only one side. Alternative names for these resonances are "leaky pseudo-Stoneley resonances," and also "Junger-type resonances," and they appear near coincidence. At their inception, and for the steel in Fig. 11, they have a phase-velocity of $0.88c_1$, which ultimately increases to c_1 at coincidence, at which point they are essentially dissipated. In the vicinity of the coincidence frequency where they occur, these two families seem to be the same, but they really have different origins.[22] This point can be verified by calculating the responses of shells to incident pulses at coincidence, in the late-time region. This excludes the broader flexural family (A_0) which dissipates faster in time, and permits the extraction of the associated group velocities from the resonance half-widths, of the Junger-type family, as was reported earlier.[29] A more detailed description and study of the partial-wave analysis that leads to Fig. 11 and these results, will appear elsewhere. Items (viii)–(xii) of Sec. I, although not used here, have been used in past resonance studies[8-10], and will be used in future ones.

III. CONCLUSIONS

The present paper examines the features in the scattering cross sections of air-filled spherical steel shells in water in the band $0 < k_1 a < 500$. The resonance features are then associated with the Lamb waves propagating in the shell material, and with other external circumferential waves propagating in the outer fluid. The presence of circumferential waves in the inner fluid does not manifest itself appreciably in the scattering cross sections. Having these resonance responses it is not hard to work backwards,[9] and be able to identify various properties of the scatterer such as its overall dimension, thickness, and material composition. For example, knowledge of the location of the large lobe that develops at the (nondimensional) coincidence frequency, x, for which $xt \sim 1$, immediately gives the relative shell thickness t.

Our analysis is based on an exact three-dimensional elasticity methodology that we described in Refs. 5 and 6, initially implemented there, and continued here. This methodology is ideal to reliably analyze any scattering problem pertaining to insonified shells fluid loaded on their inner and outer surfaces, particularly at low frequencies. This approach never misses any of the many effects present in the scattering process whether they are due to curvature, fluid loading, thickness resonances, or to choice of frequency band.

There is no need to analyze or interpret resonance features in shell cross sections by means of plate waves or plate vibrational theories, whether these are fluid loaded on one or two sides, or placed in a vacuum. The tendency to do that has been quite popular, and it has included ourselves (cf. Fig. 4, Ref. 5). However, at present, we realize that it only obscures the issues and introduces errors. It is clear from the present study that only the 3-D elasticity formulation of Refs. 5 and 6 accounts for all possible shell effects. Next best, is the use of a shell theory approximation[27,28] which will be accurate at least up to the coincidence frequency. As we saw in Fig. 7, such an approach can still extract the curvature effects responsible for the high values of the phase velocities along the A_0 and S_0 branches at low frequencies. (We repeat that the branch we have called A_0 already contains the fluid-loading effects within it.) The basic explanation is that above coincidence there is an A_0 (Lamb) wave in the shell and also a corresponding A_0 wave in the fluid, which is transmitted to it by the motion of the shell. Below coincidence, the A_0 (Lamb) wave in the shell is turned off or ceases to be excited, while its counterpart in the fluid does not. This counterpart has to account for the presence of the surrounding fluid, since without it, it would have no place to propagate. Thus what has been termed as a (*plate*) A wave (that "accounts" for the fluid loading) emerges in a natural way from the present methodology which obviously *always* accounts for the fluid loading on the (curved) *shell*. We remark that the present exact three-dimensional methodology is also available for layered shells.[3] This formulation also leads to the generation of exact dispersion plots for the phase velocities of the various types of Lamb waves propagating on fluid-loaded spherical shells. This generalizes early plate results,
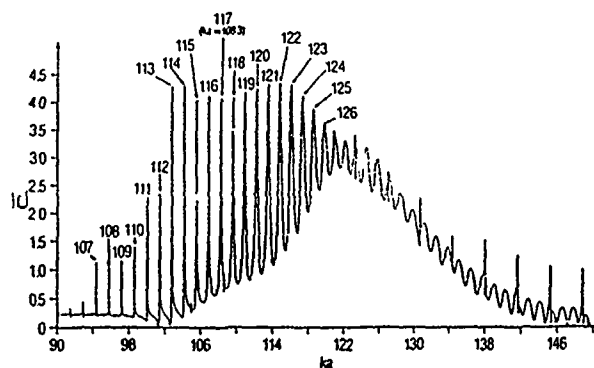

FIG. 11. Detail of the resonance response of a steel spherical shell of (relative) thickness $h/a \sim 1\%$, air filled, and submerged in water, in the band $90 < k_1 a < 150$ in the vicinity of the coincidence frequency, at which the strong flexures are seen to develop. The resonance peaks are labeled/numbered by the partial-wave analysis described in the text

such as those in Fig. 26 of Ref. 12 (or Fig. 4, Ref. 5), and discourages possible future attempts to interpret resonance features in shell cross sections by plate waves or results. We have favorably compared dispersion plots obtained by the present exact methodology and those based on the Donnell[27] shell equations (Fig. 7). We have studied a large-amplitude thickness resonance effect present in shells at relatively high frequencies. Since calculations are rarely carried out to very high frequencies (viz., $x \sim 500$ and beyond), we suspect that it was precisely for that reason that it had remained unnoticed. The present broad band calculations exhibited here have brought it into the open. The location of this thickness resonance can be predicted by Eqs. (5a) and (5c), which rest on resonance conditions of the simple type: $h = \lambda$, or $h = \lambda_d/2$, respectively. A third possible resonance condition (viz., $\lambda_s = h$) examined in this regard, does not seem to agree with the numerical calculations we have performed and displayed in Fig. 9. However, these calculations (cf. Fig. 9) do confirm the predictions of both Eqs. (5a) and (5c) within acceptable accuracy. It also follows that if calculations were to be performed in even broader frequency bands (i.e., $x > 500$) than shown here, one would be able to note higher-order thickness resonance effects of the types discussed here, caused by the overtones associated with multiples of the appropriate wavelengths. We have *illustrated* (in Fig. 6, bottom) that the resonance-isolation process typical of the RST can be very clearly and accurately accomplished over the entire spectrum by the suppression of a "modified" background that will be the subject of a later detailed study. Furthermore, by means of a partial-wave analysis, we have identified the basic types of resonance features present in the resonance response of a submerged steel shell in the vicinity of its coincidence frequency, and established their connection with the underlying surface waves. We remark in closing that the features in the cross-section of any submerged shell, as obtained from an incident cw waveform, are related to those occurring when the incidence is pulsed. For example, an energetic sinusoidal pulse of short duration incident on a shell will backscatter a pressure response that will reproduce the (steady state) form function $|f_\infty(x)|$ that was obtained for cw incidences. For this to occur, the carrier frequency x_0 of the incident pulse should coincide with one of the shell resonances $x^{(r)}$. This replication of the response will be more evident for frequencies below that carrier frequency. Conversely, for long incident pulses (say, having a delta function centered around x_0 for spectrum), the amplitude of the scattered pressure field will reproduce the portion of $|f_\infty(x)|$ near a shell resonance provided that $x_0 = x^{(r)}$. In other words, long incident cw pulses with $x_0 = x^{(r)}$, will excite individual resonances $x^{(r)}$ in the target. These ideas can all be extracted from the filter-type relation

$$rp_{sc}(\tau') = \frac{1}{2\pi} \int_{-\infty}^{+\infty} f_\infty(x') P_{\text{inc}}(x') e^{-ix'\tau'} dx', \quad (6)$$

which gives the scattered pressure in the pulsed case, in terms of the form function in the steady-state case, and the spectrum of the incident pulse. In this later case, knowledge of the transient vibration of the shell[30] becomes critical.

[1] R. Goodman and R. Stern, "Reflection and transmission of sound by an elastic spherical shell," J. Acoust. Soc. Am. 34, 338–344 (1962).

[2] K. Dierks and R. Hickling, "Echoes from hollow aluminum spheres in water," J. Acoust. Soc. Am. 41, 380–393 (1967); also, R. Hickling, "Analysis of echoes from a hollow metallic sphere in water," J. Acoust. Soc. Am. 36, 1124–1137 (1964).

[3] G. Gaunaurd and A. Kalnins, "Resonances in the sonar cross-sections of (coated) spherical shells," Int. J. Solids Struct. 18, 1083–1102 (1982).

[4] G. Gaunaurd and D. Brill, "Acoustic spectrogram and the complex-frequency poles of a resonantly excited elastic shell," J. Acoust. Soc. Am. 75, 1680–1693 (1984).

[5] V. Ayres, G. Gaunaurd, C. Tsui, and M. Werby, "The effects of Lamb waves on the sonar cross-sections of elastic spherical shells," Int. J. Solids Struct. 23, 937–946 (1987).

[6] G. Gaunaurd and M. F Werby, "Lamb and creeping waves around submerged spherical shells resonantly excited by sound scattering," J. Acoust. Soc. Am. 82, 2021–2033 (1987).

[7] M. Werby and G. Gaunaurd, "Transition from soft to rigid behavior in scattering from submerged elastic shells," Acoust. Lett. 9, 89–93 (1986).

[8] G. Gaunaurd and M. Werby, "Acoustic resonance scattering by submerged elastic shells," Appl. Mech. Rev. 43, 171–208 (1990) (and references therein).

[9] (a) G. Gaunaurd, "Resonance acoustic scattering from underwater elastic bodies," in *Elastic Wave Propagation*, edited by M. McCarthy and M. Hayes (North Holland/Elsevier, Amsterdam, 1989), pp. 335–347. (b) G. Gaunaurd, "Elastic and acoustic resonance wave-scattering," Appl. Mech. Rev. 42, 143–193 (1989) (and references therein).

[10] D. Brill and G. Gaunaurd, "Resonance theory of elastic waves ultrasonically scattered from an elastic sphere," J. Acoust. Soc. Am. 81, 1–21 (1987).

[11] I. Viktorov, *Rayleigh and Lamb Waves* (Plenum, New York, 1967).

[12] L. Brekhovskikh, *Waves in Layered Media* (Academic New York, 1960), Chap. 1.

[13] T. N. Grigsby and E. Tajchman. "Properties of Lamb waves relevant to the ultrasonic inspection of thin plates," IRE Trans. Ultrason. Eng. UE-8, 26–33 (1961).

[14] M. Redwood, *Mechanical Waveguides* (Pergamon, New York, 1960), Chaps. 2 and 3.

[15] J Achenbach. *Wave Propagation in Elastic Solids* (North Holland, New York. 1973), Chap. 5.

[16] W Ewing, W. Jardetzky, and F. Press, *Elastic Waves in Layered Media* (McGraw-Hill, New York, 1957), Chap. 4.

[17] R. Bunney, R. Goodman, and S. Marshall, "Rayleigh and Lamb waves on cylinders." J. Acoust. Soc. Am. 46, 1223–1233 (1969).

[18] G. Gaunaurd and M. F. Werby. "Resonance response of submerged acoustically excited thick and thin shells," J. Acoust. Soc. Am. 77, 2081–2093 (1985).

[19] G Gaunaurd, J Barlow, and H Ueberal. "Suppression of resonant modes from the backscattered echoes from acoustically coated air-filled cylindrical shells in water," Proc. of IV (Hydroacoustic) Symposium on Ship-Related Acoustical R&D Vol. 1-B, pp. 189–218. Monterey, CA, 1979 (ONR-sponsored, invited).

[20] N. D. Veksler, *Information Analysis in Hydroelasticity* (Academy of Sciences Estonian SSR, Tallinn–Valgus, 1982) (in Russian; NISC Translation No. 6902, of 8 Feb., 1983).

[21] N. D Veksler, *Resonance Scattering in Hydroacoustics* (Academy of Sciences of Estonian SSR, Cybernetics Institute, Valgus–Tallinn, 1984) (in Russian; NISC Translation No. 7849, of 27 Aug., 1985).

[22] M. Talmant et al., "Lamb waves and fluid-borne waves on water-loaded, air-filled thin spherical shells," J. Acoust. Soc. Am. 86, 278–289 (1989).

[23] G. S. Sammelmann et al., "The acoustic scattering by a submerged spherical shell I: Bifurcation of the dispersion curve for the spherical Lamb wave," J. Acoust. Soc. Am. 85, 114–123 (1989).

[24] L. Cremer and M. Heckl, *Structure-Borne Sound* (Springer, New York, 1973), p. 408.

[25] A. Schoch, "The transmission of sound through plates" (in German) Acustica 2 (1), 1–17 (1952).

[26] F. A. Firestone, Nondestruc. Test. 7 (2) (1948).

[27] M. Junger and D. Feit, *Sound, Structures and their Interaction* (MIT, Cambridge, MA, 1986), 2nd ed., p. 217.

[28] L. H. Donnell, "Stability of thin-walled tubes under tension," NACA Tech. Rep. No. 479, National Advisory Committee on Aeronautics, Washington, DC (1933).

[29] M. F. Werby and H. Ali, "Time-domain solution from the frequency domain... ," in *Computational Acoustics* (Elsevier Science, North Holland, Amsterdam, 1990), Vol. 2, pp. 133–148.

[30] H. Kraus and A. Kalnins, "Transient vibrations of thin elastic shells," J. Acoust. Soc. Am. 38, 994–1002 (1965).